PNAS RESEARCH ARTICLE | CELL BIOLOGY

# Lysosome-targeted multifunctional lipid probes reveal the sterol transporter NPC1 as a sphingosine interactor

Janathan Altuzar[a], Judith Notbohm[a], Frank Stein[b], Per Haberkant[b], Pia Hempelmann[a], Saskia Heybrock[c], Jutta Worsch[a], Paul Saftig[c], and Doris Höglinger[a,1]

Edited by Benjamin Cravatt, The Scripps Research Institute, La Jolla, CA; received August 12, 2022; accepted January 31, 2023

**Lysosomes are catabolic organelles involved in macromolecular digestion, and their dysfunction is associated with pathologies ranging from lysosomal storage disorders to common neurodegenerative diseases, many of which have lipid accumulation phenotypes. The mechanism of lipid efflux from lysosomes is well understood for cholesterol, while the export of other lipids, particularly sphingosine, is less well studied. To overcome this knowledge gap, we have developed functionalized sphingosine and cholesterol probes that allow us to follow their metabolism, protein interactions, and their subcellular localization. These probes feature a modified cage group for lysosomal targeting and controlled release of the active lipids with high temporal precision. An additional photocrosslinkable group allowed for the discovery of lysosomal interactors for both sphingosine and cholesterol. In this way, we found that two lysosomal cholesterol transporters, NPC1 and to a lesser extent LIMP-2/SCARB2, bind to sphingosine and showed that their absence leads to lysosomal sphingosine accumulation which hints at a sphingosine transport role of both proteins. Furthermore, artificial elevation of lysosomal sphingosine levels impaired cholesterol efflux, consistent with sphingosine and cholesterol sharing a common export mechanism.**

protein–lipid interaction | photocrosslinking | sphingolipids | lysosomal storage diseases | organelle-targeted probes

## Significance

Diverse fatty molecules taken up by diet or generated by digestion of biological membranes rely on the lysosome for processing and further transport. Abnormal accumulation of lipids in these lysosomes is a hallmark of several rare genetic diseases but has also been observed in common neurodegenerative disorders. However, the underlying mechanism for the export of certain lipids such as sphingosine is not yet explored. Here, we present a method based on chemical functionalization of lipids which allows the prelocalization and controlled release of sphingosine and cholesterol probes in the lysosome. Using these probes, we discovered that proteins previously thought to be responsible for cholesterol transport are also involved in sphingosine export from lysosomes.

Lipid homeostasis is maintained by an intracellular network of enzymes and regulated by organelle-to-organelle communication. Within this network, the lysosome plays a central role as host for degradation, recycling, and trafficking of biomolecules such as proteins, nucleic acids, and lipids (1). Lysosomal dysfunction manifests in severe human pathologies known as lysosomal storage diseases (LSDs) which are often associated with lipid and particularly sphingolipid accumulation (2, 3).

Cholesterol is one well-studied lipid that relies on lysosomal trafficking. Dietary cholesterol reaches its target cells in plasma low-density lipoprotein (LDL) form. Upon endocytosis, LDL is hydrolyzed in lysosomes, triggering release of free cholesterol (4). Subsequently, lysosomal cholesterol is transported to the plasma membrane (PM) or endoplasmic reticulum (ER). At the ER, sterol levels are sensed, and cholesterol biosynthesis is regulated accordingly (5). Excess cholesterol is converted into cholesteryl esters for storage in lipid droplets (6). The exact mechanism of cholesterol egress from endocytic organelles to the ER or PM compartment is not fully elucidated. However, a substantial body of evidence implicates Niemann–Pick type C1 and C2 proteins (NPC1 and NPC2) in lysosomal cholesterol traffic (7–10). Aside from transporting cholesterol toward the lysosomal limiting membrane via a hydrophobic, intramolecular tunnel (11), NPC1 has further been shown to form organelle contact sites with ER-resident proteins such as ORP5 (12) or Gramd1b (13). This tethering function of NPC1 may further contribute to its importance in lysosomal cholesterol efflux from the lysosome to the ER. Alternatively, cholesterol can exit the lysosome through lysosomal integral membrane protein 2 (LIMP-2/SCARB2) which also features a hydrophobic intramolecular tunnel (14, 15).

While postlysosomal cholesterol traffic has been extensively studied (10, 16), other lipids are also degraded in the lysosome. Here, the biologically active class of sphingolipids are of interest, given that a large number of LSDs feature lysosomal sphingolipid accumulation. Glycosphingolipid (GSL) catabolism proceeds through internalization of the PM and the recycling of membrane components through the endolysosomal degradation pathway (17). Here, sphingomyelin (SM) and GSLs reach the lysosome and are degraded to form ceramides (18). In the last step of lysosomal sphingolipid catabolism, ceramides (Cer) are hydrolyzed to form sphingosine (Sph) (19), the backbone of all sphingolipids. Sph can be either recycled back into the sphingolipid biosynthetic pathway (20) or phosphorylated to form sphingosine-1-phosphate and be degraded through the actions of

Author contributions: J.A., J.N., P.S., and D.H. designed research; J.A., J.N., P. Haberkant, P. Hempelmann, and J.W. performed research; S.H. and P.S. contributed new reagents/analytic tools; J.A., J.N., F.S., P. Haberkant, P. Hempelmann, and D.H. analyzed data; and J.A., J.N., P.S., and D.H. wrote the paper.

The authors declare no competing interest.

This article is a PNAS Direct Submission.



[1]To whom correspondence may be addressed. Email: doris.hoeglinger@bzh.uni-heidelberg.de.

This article contains supporting information online at https://www.pnas.org/lookup/suppl/doi:10.1073/pnas.2213886120/-/DCSupplemental.

Published March 9, 2023.

sphingosine-1-phosphate lyase (SGPL1). Breakdown products of this degradation pathway can feed into the glycerolipid synthesis pathway (21). While much is known about the enzymes involved in sphingolipid catabolism, the machinery responsible for lysosomal sphingolipid export is completely unknown. This can be attributed to a lack of functional tools to investigate sphingolipids on a single-organelle and single lipid species level.

To date, several tools have been used to follow sphingolipid metabolism and localization (22, 23). Covalently labeled fluorescent lipids that contain fluorescent dyes such as fluorescein, nitrobenzoxadiazole, pyrene, and boron-dipyrromethene (BODIPY)-like structures attached to their acyl chain or head group have been reported (24, 25). However, they exhibit several drawbacks, such as aberrant membrane integration, mislocalization, and poor cell uptake (26–28). Bifunctional lipids (22, 29) on the other hand have become popular compounds used to circumvent the problems associated with fluorescent lipids. These lipids combine a photocrosslinkable diazirine group, which allows cross-linking upon short-wavelength ultraviolet (UV) illumination, with an alkyne or azide group for subsequent staining or enrichment of lipid–protein complexes. Given that these modifications are quite small in size, the modified lipids quite accurately mimic the cellular behavior of their endogenous counterparts, which has been demonstrated for lipids such as cholesterol (30), fatty acids (29), or Sph (22). One major drawback is that these lipids are rapidly metabolized after addition to cells, giving rise to a host of modified lipid metabolites. This hinders the study of small bioactive sphingolipids such as Sph, which, due to their potent signaling properties, is rapidly metabolized or degraded by the cell (22). To circumvent rapid metabolism, trifunctional lipids have been developed, where photocleavable protection (or "cage") groups allow for equal loading of all cells before the active lipid probes can be released by a flash of longer-wavelength UV light (31, 32). This strategy achieves a rapid burst of the lipid probe with high spatial and temporal resolution. Additionally, using an inherently fluorescent cage group such as coumarin allows the visualization of the probe's localization before uncaging. However, it was shown that the cage group associates nonselectively with all internal membranes and therefore artificially mislocalizes the lipid of interest (32). As such, trifunctional lipids are not well suited to study questions related to interorganellar transfer. However, an additional strategy has recently been described to overcome this technical problem and achieves organelle specificity. Here, slight chemical modifications to the coumarin cage group led to their prelocalization to different organelles such as the plasma membrane, mitochondria, or lysosomes (33, 34). So far, organelle targeting of caged lipids has only been applied to nonfunctionalized or deuterated lipids (34–36).

In this study, we combine the advantages of trifunctional and organelle-targeted lipids to create versatile tools for the visualization of single lipids and for the identification of their protein interactome at the single-organelle level. We synthesized and applied lysosome-targeted photoactivatable and cross-linkable (pac) sphingosine (lyso-pacSph) and cholesterol (lyso-pacChol) to address outstanding questions regarding postlysosomal sphingolipid trafficking and metabolism. These multifunctional tools allow us to i) prelocalize sphingosine and cholesterol probes into lysosomes, ii) screen for lysosomal protein–lipid interactors, iii) follow their postlysosomal metabolic fate by thin layer chromatography (TLC), and iv) visualize time-resolved lipid localization by confocal microscopy. We demonstrate the suitability of such a design by using lyso-pacSph to identify lysosomal interactors and potential lysosomal membrane transporters of Sph and show a surprising commonality in lysosomal Sph and cholesterol export routes.

## Results

**Synthesis and Characterization of Lysosome-Targeted pacSphingosine and pacCholesterol Probes.** We have designed lyso-pacSph and lyso-pacChol to feature four functionalities: i) a photoactivatable diazirine ring for UV-dependent photocrosslinking, ii) a clickable alkyne group which allows postcrosslinking functionalization of the lipid with fluorophores or biotin (29), and a iii) photocleavable protecting group (cage) (32) equipped with a iv) tertiary amine lysosomal targeting group. This targeting group is retained in the acidic environment of late endosomes and lysosomes in its protonated form (37). This design ensures that all probe molecules are delivered to lysosomes before a flash of light ("uncaging") releases the active lipid species. We initially synthesized the lysocoumarin caging group (**4**) from a previously described precursor (34) and added a linker to incorporate the targeting group. Next, we coupled this cage to commercially available pacSph and pacChol (30) through respective carbamate and carbonate linkages in order to afford the lyso-pacSph (**5**) and lyso-pacChol (**6**) with 99% and 96% yield, respectively (Fig. 1*A*).

Following synthesis of the compounds, we investigated cellular uptake of these probes by live-cell confocal microscopy using the inherent fluorescence of the coumarin cage group. We found that both probes were readily taken up by HeLa cells over a wide range of concentrations from 750 nM to 10 μM after 60 min of labeling (*SI Appendix*, Fig. S1*A*). Interestingly, lyso-pacChol showed an immediate vesicular localization at all investigated concentrations, whereas lyso-pacSph was distributed to all internal membranes. To improve the subcellular localization of lyso-pacSph, we next varied probe-free incubation ("chase") times ranging from 0 min to 18 h (*SI Appendix*, Fig. S1*B*). Lyso-pacChol remained located in vesicles at all chase times, but lyso-pacSph required longer chase times with exclusive vesicular localization obtained after 18 h of chase. Using these optimized, 18-h chase conditions for both probes, we then investigated whether the vesicles stained with lyso-pacSph and lyso-pacChol were indeed lysosomes. We found that the fluorescent coumarin pattern of the lysoprobes overlapped completely with LysoTracker™ signal as quantified using Pearson's correlation coefficient (PCC) with values of 0.84 or higher (Fig. 1 *B* and *C*).

Given that long chase times were required to achieve optimal lysosomal localization of lyso-pacSph, we next investigated the stability of the lysoprobes to withstand the activities of lipases and esterases found in the lumen of lysosomes prior to their uncaging. To this end, we pulsed and chased HeLa cells with both lysoprobes for up to 24 h, extracted the lipids, and added a commercially available fluorophore to the alkyne group by means of click chemistry. TLC analysis revealed that no additional bands appeared during 24 h of chase times (*SI Appendix*, Fig. S1 *C* and *D*), confirming that the lysoprobes are inert and not subject to cellular metabolism while in their caged form. To evaluate the photocleavage efficiency of the lysoprobes, we performed uncaging experiments of both lysoprobes in aqueous solution with increasing duration of UV irradiation (405 nm). Here, TLC analysis showed that 60 to 90 s were sufficient to photocleave ("uncage") almost all probe molecules and release the active lipid species (*SI Appendix*, Fig. S1 *E* and *F*). Having optimized the uncaging step, we next studied the metabolic consequences of uncaging the lipid probes in living cells. TLC analysis of lyso-pacSph (Fig. 1*D*) and lyso-pacChol (Fig. 1*E*) again showed that incubation without uncaging

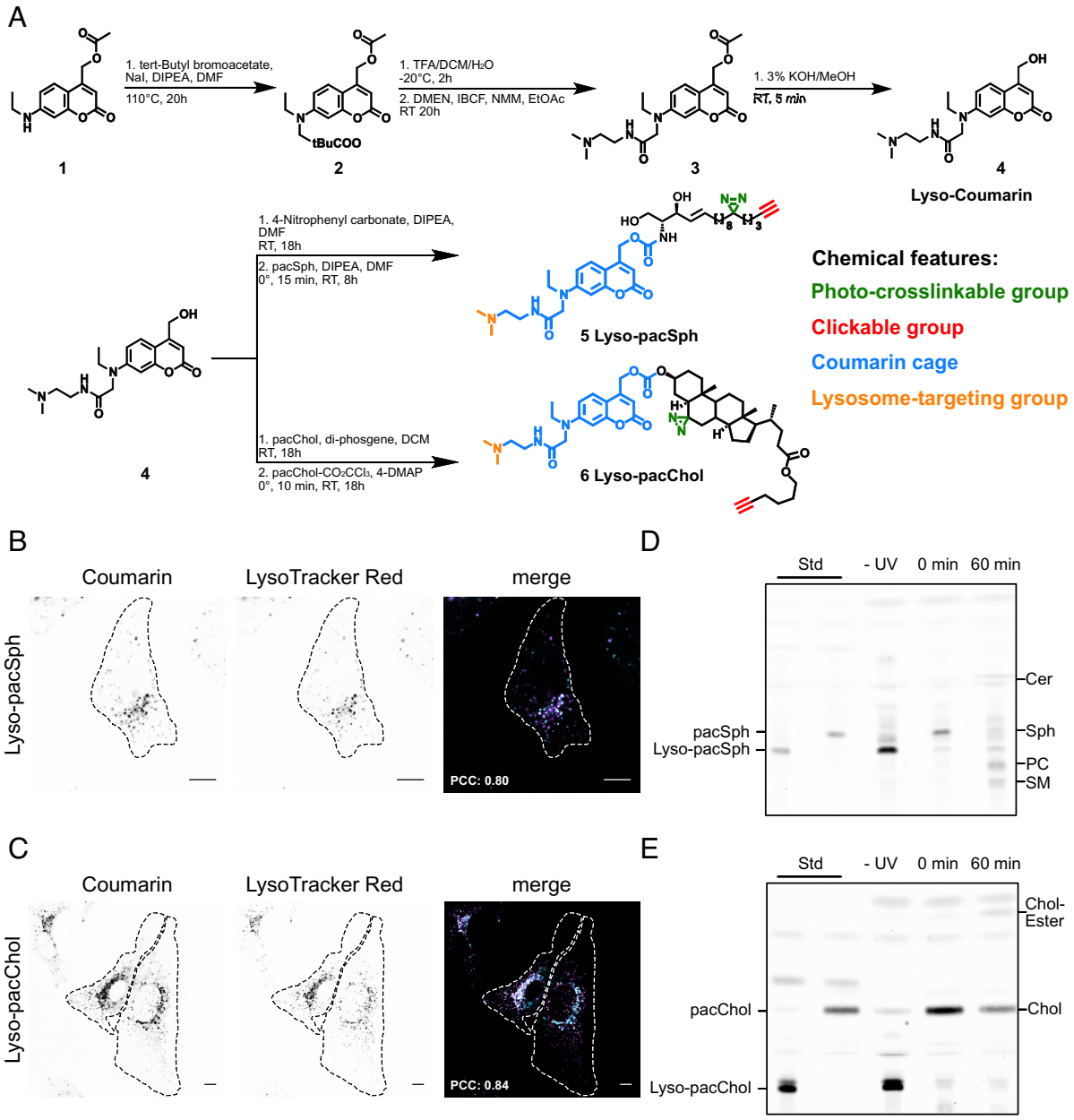


**Fig. 1.** Synthesis and characterization of lysosome-targeted probes. (*A*) Synthesis of lysosome-targeted coumarin (lysocoumarin, 4), lysosome-targeted pacSphingosine (lyso-pacSph, 5), and lysosome-targeted pacCholesterol (lyso-pacChol, 6). Annotation of the functional groups by color-coded legend. (*B* and *C*) Lysosomal localization of lysoprobes. Confocal images of coumarin fluorescence in HeLa cells pulsed with lyso-pacSph or lyso-pacChol (10 μM) for 1 h and 45 min, respectively, chased overnight, and incubated with LysoTracker Red (100 nM) 30 min previous to imaging. (Scale bar, 10 μm.) Lysoprobe: cyan and LysoTracker Red: magenta (*D* and *E*) Thin layer chromatography of HeLa cells pulsed with lyso-pacSph or lyso-pacChol (10 μM) for 1 h and 45 min, respectively, chased overnight, harvested immediately, and/or irradiated with a 405-nm UV light for 90 s and further incubated at 37 °C for indicated times. Cellular lipids were extracted, labeled with 3-azido-7-hydroxy coumarin, spotted, and developed on a silica plate.

(–UV) does not release the active (pac) lipid species, whereas immediately after uncaging (0'), only the active species pacSph and pacChol could be detected. When incubating a further 60 min after uncaging (60'), however, the modified lipids were further incorporated into their respective downstream metabolites. Lyso-pacSph was converted to ceramide (Cer), sphingomyelin (SM), and to a significant degree to phosphatidylcholine (PC), a product of the sphingosine-1-phosphate lyase (S1PL)-dependent breakdown pathway (identification of the bands with their respective standards in *SI Appendix*, Fig. S1*G*). In further experiments, to avoid the incorporation of the labeled sphingosine backbone into abundant glycerolipids, a SGPL1-deficient HeLa cell line (as shown in refs. 38 and 22) was employed, thereby limiting experimental readouts to lipid species containing the sphingosine backbone. Lyso-pacChol on the other hand was metabolized fairly slowly and to only one further species, a cholesterol ester (Fig. 1*E*). Therefore, all further experiments using lyso-pacChol were carried out in HeLa wild type (WT) cells. Together, these data showed that the sphingosine and cholesterol analogs released inside lysosomes closely resemble their endogenous counterparts and readily participate in their respective metabolic pathways in accordance with previous studies using trifunctional sphingosine (32) and bifunctional cholesterol (13).

**Suitability of Lyso-pacSph and Lyso-pacChol to Investigate Lysosomal Protein–Lipid Interactions.** We next investigated the usefulness of these stable lysosome-targeted probes in studying subcellular protein–lipid interactions. To this end, we compared

the uncaged and therefore globally distributed pacSph and pacChol probes (22, 30) with our newly synthesized lysoprobes and first visualized their subcellular localization in a workflow consisting of metabolic labeling, uncaging, and cross-linking photoreactions, followed by fixation and staining of their localization by click reaction to a fluorophore. There, we could indeed show that the uncaged versions globally distributed throughout the cell, while the lysoprobes remain confined to the lysosomes (*SI Appendix*, Fig. S2 *A* and *B*, quantified in *SI Appendix*, Fig. S2 *C* and *D*). Such conditions were then employed in the analysis of proteins interacting with these probes. Again, the workflow consisted of metabolic labeling, uncaging, and cross-linking but followed by click reaction to streptavidin and enrichment by streptavidin-mediated immunoprecipitation (Fig. 2*A*). In this way, we could

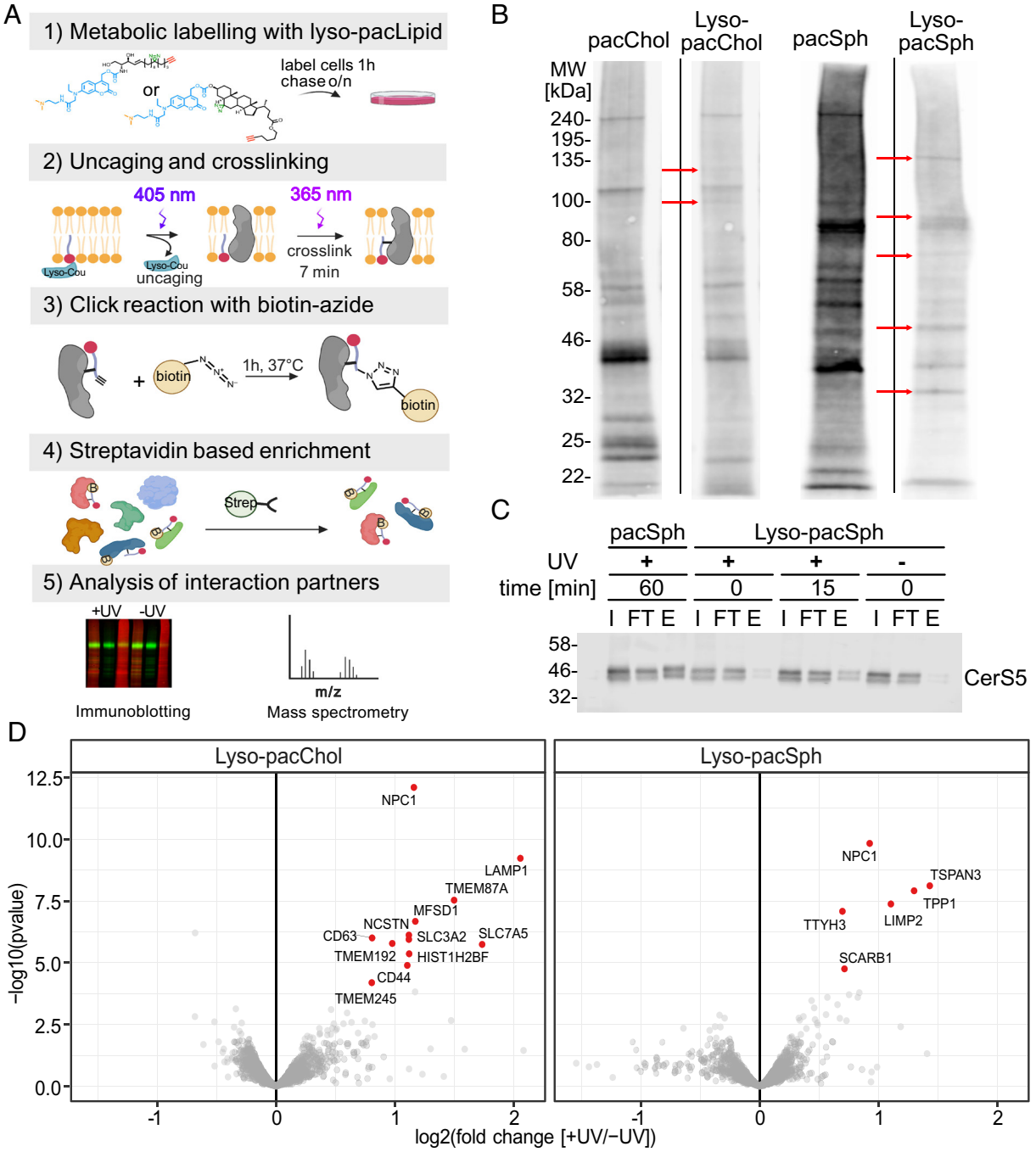


**Fig. 2.** Application of lyso-pacChol and lyso-pacSph for identification of protein–lipid interactions. (*A*) Scheme illustrating the workflow used to capture protein interactors. Created with Biorender.com (*B*) Differential identification of proteins cross-linked to pacChol (10 μM) vs. lyso-pacChol (10 μM) and pacSph (1 μM) vs. lyso-pacSph (5 μM). Biotinylated protein–lipid complexes were visualized using fluorescently labeled streptavidin. Proteins identified with lysoprobes but not with globally distributed probes are marked with red arrows. (*C*) Time-dependent identification of FLAG-tagged ceramide synthase 5 (CerS5) by lyso-pacSph compared to globally distributed pacSph. HeLa SGPL1$^{-/-}$ cells were labeled with lyso-pacSph (5 μM) or pacSph (2 μM for 1 h) uncaged and either cross-linked immediately or incubated 15 min before cross-linking and subjected to the workflow in (*A*) featuring cross-linking (+UV) or no cross-linking (−UV) steps. The inputs (I, 10%), flow-throughs (FT, 10%), and eluates (E, 100%) were immunoblotted against FLAG tag. (*D*) Chemoproteomic analysis of lyso-pacChol (10 μM) and lyso-pacSph (5 μM) interactors. Volcano plot showing the results of a differential abundance analysis using the limma package (moderated *t* test and *P* values estimated by the fdrtool package) of proteins cross-linked to the respective probes. $Log_2$ fold change of cross-linked over noncrosslinked (*x* axis) and negative $log_{10}$ *P* values (*y* axis) of protein interactors. Hit proteins (red annotated dots) displayed a false discovery rate of ≤0.01 and a fold change of >1.5.

reveal all biotinylated protein–lipid complexes by using fluorescent streptavidin (Fig. 2*B*). As expected, the lysosomal probes gave rise to a reduced subset of cross-linked partners compared to their globally distributed counterparts. However, several bands (marked with red arrows) could only be detected using the lysosomal probes, highlighting the sensitivity of this method to capture scarce or brief interactions which would be missed when using nonprelocalized probes.

Next, we tested whether this workflow was suitable to enrich known lysosomal proteins and investigated the well-studied lysosomal cholesterol-binding proteins NPC1, LAMP1, and LIMP-2/SCARB2 by immunoblotting following streptavidin-mediated immunoprecipitation (*SI Appendix*, Fig. S3*A*). Encouragingly, all three investigated proteins could be detected in eluate ("E") fractions of both pacChol- and lyso-pacChol-treated samples, whereas only a slight background signal stemming from unspecific binding to streptavidin beads could be detected in the –UV samples, where the photocrosslinking step was omitted. This supports that the established workflow can specifically detect lysosomal protein–lipid interactions.

As a further challenge to the spatiotemporal resolution, we next studied the availability of lysoprobes to nonlysosomal proteins. To this end, we investigated whether lyso-pacSph was able to interact with an ER-resident protein, ceramide synthase 5 (CerS5, Fig. 2*C*). Given that Sph is a substrate of CerS5, we unsurprisingly detected CerS5 in the eluate fractions of samples treated with the globally distributed pacSph. However, samples collected immediately upon uncaging of lyso-pacSph (0 min) did not reveal CerS5 in the elution fraction, further supporting the exquisite time sensitivity of this assay. However, when a 15-min incubation was added upon uncaging, CerS5 could once again be detected in the elution fraction, indicating a successful transport of the lyso-pacSph probe to the ER. Together, these data highlight the suitability of the lysoprobes to specifically detect lipid-interacting proteins with a high spatial and temporal control.

**Chemoproteomic Profiling of Lyso-pacSph and Lyso-pacChol.** Next, we set out to explore lysosomal interactors of Sph and cholesterol in an unbiased fashion. At 0 min after uncaging to ensure maximum lysosomal localization, we again used the lysoprobes in the workflow based on streptavidin-mediated immunoprecipitation, but now, we analyzed the eluates by tandem mass tag (TMT)–based quantitative proteomics. Comparison of cross-linked (+UV) with nonirradiated (–UV) samples gave a small subset of proteins which passed the strict threshold of a false discovery rate (FDR) below 0.01 and a fold change of 1.5 (Fig. 2*D*, a list of hit proteins in *SI Appendix*, Fig. S4 *A* and *B*). For lyso-pacChol-treated cells, we found known lysosomal cholesterol interactors such as NPC1 and LAMP1 (39, 40) among 12 candidate hits. Only six of those had been previously identified using the nonprelocalized pacChol probe (30). Lyso-pacSph-treated samples gave only six proteins. Two of those (SCARB1 and TTYH3) are annotated as plasma membrane proteins. Among the other four candidates, we found two cholesterol transporters NPC1 and LIMP-2/SCARB2 as potential Sph interactors. We next validated the Sph interaction with NPC1 and LIMP-2/SCARB2 by immunoprecipitation and western blot analysis and indeed found that both probes were efficiently pulled down with both the globally distributed pacSph and lyso-pacSph, again only showing slight background staining in conditions where the cross-linking step was omitted (*SI Appendix*, Fig. S3*B*). To our surprise, the amount of NPC1 and LIMP-2/SCARB2 present in the eluate fraction was higher when pacSph was employed, suggesting more efficient cross-linking of the globally distributed probe. This could stem from differences in lysosomal concentrations of the active pacSph in both conditions or a potential contribution of additional binding of downstream (sphingo)lipid metabolites that are present in much higher fractions in the pacSph condition compared to the uncaged lyso-pacSph. As a negative control, we included the most abundant lysosomal membrane protein LAMP1 which was not detected in the eluate fractions of pacSph or lyso-pacSph-treated cells (*SI Appendix*, Fig. S3*B*), highlighting the specificity of the detected interactions with NPC1 and LIMP-2/SCARB2. Performing in-lysate competition experiments using pacSph with increasing concentrations of natural Sph or cholesterol (*SI Appendix*, Fig. S3 *C–F*), we could further show that the NPC1-Sph cross-linking detected by our workflow was sensitive to competition with endogenous Sph, where a 10-fold excess (500 μM) resulted in a markedly decreased cross-linking (*SI Appendix*, Fig. S3*C* and quantified in *SI Appendix*, Fig. S3*D*), whereas competition with up to 50-fold excess cholesterol (2.5 mM) could only partially displace the detected NPC1–Sph cross-linking (*SI Appendix*, Fig. S3*E* and quantified in *SI Appendix*, Fig. S3*F*). These data provide a hint that Sph and cholesterol could share a common binding site, and the fact that even large excess of cholesterol only partially disrupted NPC1–Sph binding could point toward a scenario where Sph interacts preferentially with NPC1.

**Metabolic Fate of Lysosomal Cholesterol and Sphingosine.** Next, we were curious to study the metabolic fate of the lysoprobes and, in particular, whether the newly identified Sph interactors NPC1 and LIMP-2/SCARB2 affected the kinetics of postlysosomal cholesterol and Sph metabolism. To this end, we performed pulse–trace experiments in which we liberated both lysoprobes by uncaging ("pulse") in WT, NPC1$^{-/-}$ (41) and LIMP-2/SCARB2$^{-/-}$ HeLa cells and analyzed the probe metabolites after different times after uncaging ("trace") by thin layer chromatography. Of note, this experiment does not feature a cross-linking step, and therefore, the time resolution is decreased as additional minutes are needed to collect cells and perform lipid extraction. As expected, lyso-pacChol-labeled cells showed a time-dependent increase in cholesterol ester (Fig. 3*A*). This progressive incorporation of cholesterol into cholesterol esters is severely reduced and delayed in NPC1$^{-/-}$ and LIMP-2/SCARB2$^{-/-}$ HeLa cells (Fig. 3*A* and quantified in Fig. 3*B*) in line with previous studies showing a lysosomal export defect of cholesterol under these conditions (15, 42). WT cells labeled with lyso-pacSph not only showed extremely rapid metabolic conversions (Fig. 3*C*) where the precursor was incorporated into higher sphingolipids such as ceramide but also degraded via the S1PL pathway, yielding a small portion of labeled phosphatidylcholine at the earliest time point. Conversely, NPC1$^{-/-}$ cells showed a delayed decrease in Sph levels compared to WT cells consistent with a potential transport defect. LIMP-2-deficient cells, on the other hand, only featured slightly delayed Sph export kinetics (Fig. 3*C*, quantified in Fig. 3*D*). Together, loss in lysosomal proteins NPC1 and LIMP-2/SCARB2 significantly impacted postlysosomal cholesterol metabolism, whereas Sph metabolism was found to generally proceed much faster and depend more on NPC1 than LIMP-2/SCARB2.

**Lysosomal Egress and Subcellular Localization of Sphingosine and Cholesterol across Organelles in NPC1 and LIMP-2/SCARB2-Deficient Cells.** Next, we visualized the time-dependent changes in subcellular localization of lysoprobes by confocal microscopy in order to investigate whether lysosomal egress was indeed delayed as suggested by the TLC studies. To this end, we took advantage of the versatility of the clickable group to attach a fluorophore as

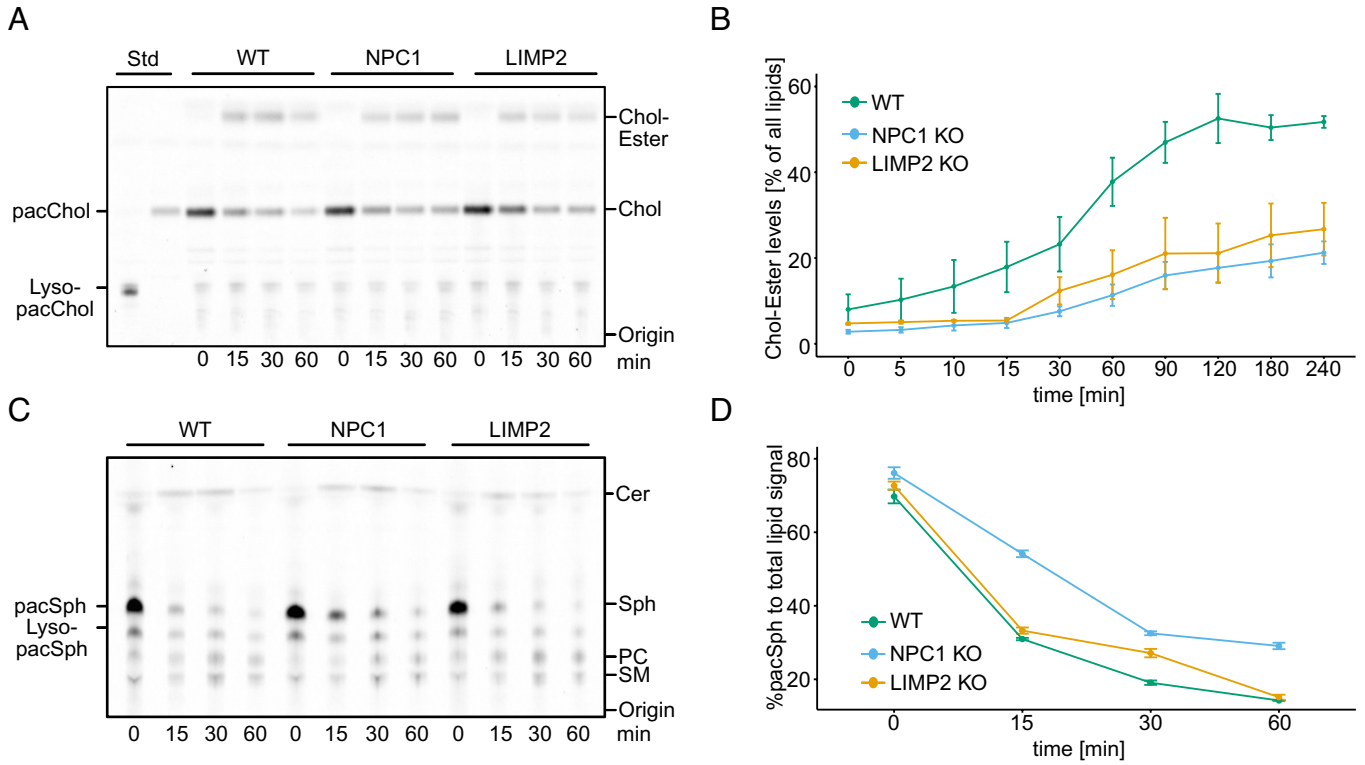


**Fig. 3.** Lyso-pacChol and lyso-pacSph metabolism in WT, NPC1 KO, and LIMP2 KO cells by TLC. (*A*) Postlysosomal metabolism of lyso-pacChol (*A*). HeLa WT, NPC1 KO, or LIMP-2/SCARB2 KO cells were labeled with lyso-pacChol (10 μM) or for 45 min and chased overnight. Upon uncaging, cells were chased and lipids extracted at indicated times, clicked with 3-azido-7-hydroxycoumarin, and visualized by TLC. (*B*) Quantification of cholesterol esterification in WT, NPC1, and LIMP2-deficient HeLa cells. The intensity of the ester corresponding to pacChol ester divided by the sum of pacChol and pacChol ester is displayed as percentage. (*C*) TLC analysis of lipid metabolites arising from incubation of HeLa WT, NPC1 KO or LIMP-2/SCARB2 KO cells with lyso-pacSph (10 μM) for 1 h, overnight chase, uncaging and extraction at the indicated times. (*D*) Quantification of lysosomal sphingosine (Sph) export in WT, NPC1, and LIMP2-deficient HeLa cells. Sph is readily metabolized not only to ceramide (Cer) and sphingomyelin (SM) but also to phosphatidylcholine (PC) via the SGPL1 breakdown pathway. Intensity of the Sph is expressed as percentage compared to the sum of all labeled lipids. Data are shown as mean of three independent experiments ± SE.

another reporter molecule in pulse–trace experiments (Fig. 4 *A* and *B*). In WT cells labeled with lyso-pacChol, a predominantly lysosomal localization was visible at 0 min, followed by staining of internal membranes, the Golgi apparatus, and the plasma membrane after 30 min. At 60 to 90 min, some of the probes localized to lipid droplets (colocalization with respective organelle markers in *SI Appendix*, Fig. S5*A*) likely in the form of cholesterol esters. In accordance with previous studies (43, 44), cells lacking NPC1 showed a significant retention of the lyso-pacChol probe in lysosomes for up to 90 min (*SI Appendix*, Fig. S5*B*). LIMP-2/SCARB2$^{-/-}$ cells on the other hand showed an intermediate phenotype with internal membranes stained with similar kinetics as in WT cells, yet some lysosomes were visible throughout the 90-min time course (*SI Appendix*, Fig. S5*C*, quantification in Fig. 4*C*). This could potentially point toward different populations of lysosomes, one population with a functional cholesterol export route (arguably via NPC1 to the ER) and a smaller population with defective cholesterol export mediated by LIMP-2/SCARB2. Investigating a double NPC1/LIMP-2 knockout (KO) cell line gave again strong lysosomal staining over the entire time course (*SI Appendix*, Fig. S5*D*), and the quantification of lysosomal colocalization (Fig. 4*C*) showed comparable correlation coefficients as in the single NPC1$^{-/-}$ line, supporting again that the main export route of cholesterol from lysosomes depends on NPC1.

We next utilized lyso-pacSph to study the yet unexplored lysosomal export of Sph (Fig. 4*B*, colocalization in *SI Appendix*, Fig. S6). In WT cells, Sph relocalized from lysosomes to predominantly Golgi membranes at 30 min (*SI Appendix*, Fig. S6*A*, quantified in *SI Appendix*, Fig. S6*E*), while at later time points, much of the initial signal intensity was lost, consistent with efflux or effective catabolism of the sphingosine probe. In NPC1$^{-/-}$ cells, a striking Sph storage phenotype was observed with lysosomes stained for the entire time course and only a small part of the probe localizing to other internal membranes (*SI Appendix*, Fig. S6*B*). This observation was corroborated by a high Pearson coefficient throughout the time course (Fig. 4*D*). LIMP-2/SCARB2$^{-/-}$ cells, again, showed an intermediate phenotype with a partial export to internal membranes and partial storage in a small subset of lysosomes (*SI Appendix*, Fig. S6*C*). Interestingly, the double NPC1/LIMP-2 knockout cell line gave almost exclusive lysosomal localization over the entire time course (*SI Appendix*, Fig. S6*D*) with consistently high Pearson coefficient (Fig. 4*D*), pointing at a potential additive effect of both knockouts. It should be noted that this was done on CRISPR/Cas9-generated cell lines, and as such, clonal effects could play a role, in particular, for cells that have such a strong metabolic defect. Together, these data show another surprising commonality between sphingolipid and cholesterol trafficking such that the absence of previously known cholesterol transporters NPC1 and LIMP-2/SCARB2 also affects the kinetics of Sph export and that for Sph export in particular, NPC1 and LIMP-2/SCARB2 might be functioning in parallel.

**Sphingosine Transport Defect Is a Direct Consequence of NPC1 Dysfunction.** To further investigate the prominent Sph storage phenotype in NPC1-deficient cells and to exclude that the observed phenomenon was a downstream effect caused by long-term adaptation in our particular NPC1$^{-/-}$ cell line, we next evaluated pharmacological inhibition of NPC1 in WT cells

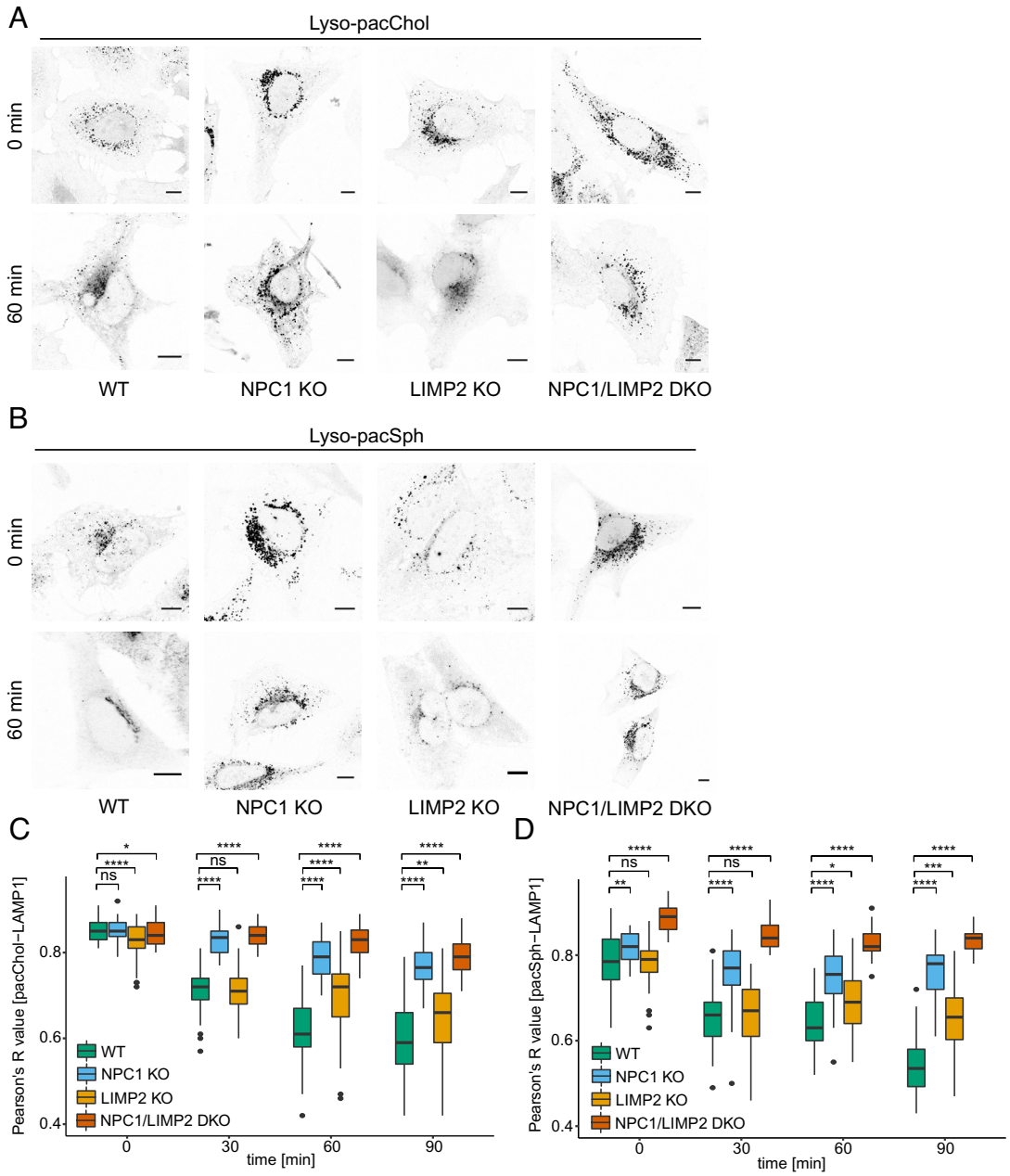


**Fig. 4.** Visualization of lysosomal lipid egress in WT, NPC1 KO, LIMP2 KO, and NPC1/LIMP2 DKO cells. Subcellular localization of lyso-pacChol (*A*) and lyso-pacSph (*B*) in WT, NPC1, LIMP2, and NPC1/LIMP2-deficient HeLa cells. Confocal images of cells labeled with lyso-pacChol or lyso-pacSph (10 μM) for 45 min and 1 h, respectively, and chased overnight. Upon uncaging, cells were chased for the indicated times, cross-linked, fixed, and functionalized with AlexaFluor 594 picolyl azide (*B*) or AlexaFluor 488 picolyl azide (*A*). (Scale bar, 10 μm.) (*C* and *D*) Quantification of lysosomal lipid egress. Pearson's R value of nonthresholded images from lipid channel vs. LAMP1 immunofluorescence calculated for each time point (n ≥ 45) using the Coloc 2 feature from Fiji (ns *P* value > 0.5, **P* ≤ 0.05, ***P* ≤ 0.01, ****P* value ≤ 0.001, and *****P* value ≤ 0.0001).

by acute treatment with U18666A. This drug has been shown to inhibit the sterol-sensing domain of NPC1 and to block cholesterol export (45). Repeating the lyso-pacSph pulse–chase experiment in the presence of U18666A showed that, again, Sph export from lysosomes was severely delayed compared to WT cells (Fig. 5*A*, quantified in Fig. 5*B*, colocalization images in *SI Appendix*, Fig. S7 *C–E*), although to a slightly lesser degree than in a genetic knockout model. For further validation, we also employed the structurally distinct NPC1 inhibitors itraconazole and posaconazole (46, 47). Export assays employing lyso-pacChol (*SI Appendix*, Fig. S8*A*, quantified in *SI Appendix*, Fig. S8*B*) revealed successful inhibition with lysosomal retention of the probe similar to the genetic knockout. Investigating Sph export under these inhibition conditions, we observed again a severe delay in export, even above levels seen in the genetic knockout (*SI Appendix*, Fig. S8*C*, quantified in *SI Appendix*, Fig. S8*D*). To challenge whether the observed Sph storage was a primary effect due to loss of NPC1 or a secondary effect created by NPC1-induced cholesterol accumulation and a potentially resulting reduced capacity of lysosomes to export Sph, we subjected NPC1$^{-/-}$ cells to starvation by growing them in lipoprotein-deficient medium. This treatment drastically reduced lysosomal cholesterol levels as revealed by filipin staining (*SI Appendix*, Fig. S7*A*, quantified in *SI Appendix*, Fig. S7*B*). Investigating lyso-pacSph efflux under these conditions revealed that Sph still remained trapped in lysosomes for the duration of the time course in the same degree as nonstarved NPC1 cells (Fig. 5*A*, quantified in Fig. 5*B*, colocalization images in *SI Appendix*, Fig. S7*F*), arguing for a direct

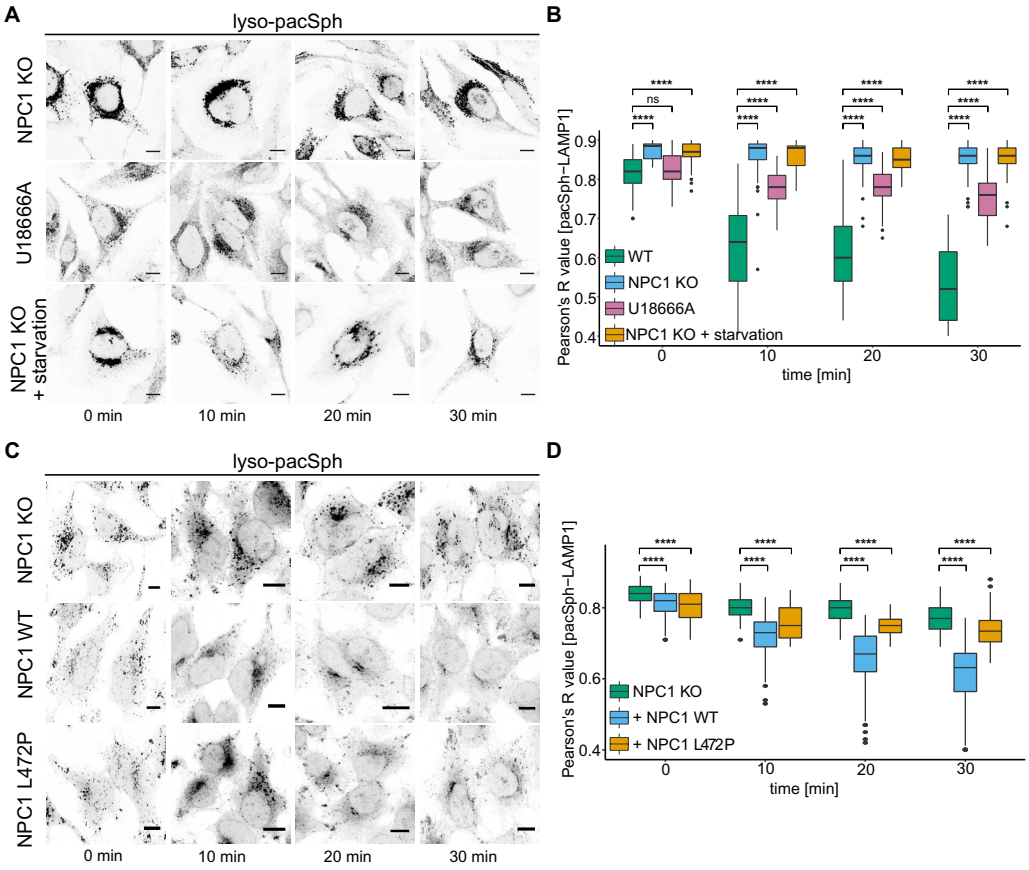


**Fig. 5.** Sphingosine accumulation is a direct effect from loss of NPC1. (*A*) Confocal images of lyso-pacSph in cellular models of NPC1. HeLa NPC1 KO cells (NPC1), HeLa WT cells treated with 0.5 μg/mL U18666A 24 h prior to imaging (U18666A), and HeLa NPC1 KO cells incubated with lipoprotein-deficient medium 48 h prior to imaging (starvation) were labeled with lyso-pacSph (1.25 μM) for 1 h and chased overnight. Upon uncaging, cells were chased from 0 to 30 min, cross-linked, fixed with methanol, and functionalized with AlexaFluor 594 picolyl azide. (Scale bar, 10 μm.) (*B*) Quantification of lysosomal lipid egress. Pearson's R value of nonthresholded images from lipid channel vs. LAMP1 immunofluorescence calculated for each time point (n ≥ 42) using the Coloc 2 feature from Fiji (ns *P* value > 0.05. (*C*) Confocal images of lyso-pacSph in cellular models of NPC1. HeLa 11ht NPC1 KO cells (NPC1 KO) with NPC1-Flag induced on an NPC1 KO background (NPC1-WT) or NPC1 (L472P)-Flag induced on an NPC1 KO background (NPC1 L472P) were labeled with lyso-pacSph (10 μM) for 1 h and chased overnight. Upon uncaging, cells were chased from 0 to 30 min, cross-linked, fixed with methanol, and functionalized with AlexaFluor 594 picolyl azide. (Scale bar, 10 μm.) (*D*) Quantification of lysosomal Sph egress in cellular models of NPC1. Pearson's R value of nonthresholded images from lipid channel vs. LAMP1 immunofluorescence calculated for each time point (n ≥ 73) using the Coloc 2 feature from Fiji (ns *P* value > 0.05 and ****$P$ value ≤ 0.0001).

role of NPC1 on Sph transport. This could either be mediated by direct trafficking of Sph through NPC1 analogous to its action in cholesterol export or by indirect action of NPC1 as a contact site tether. Previous studies showed NPC1 to be involved in creating and maintaining organelle contact sites of lysosomes with the ER (13) and that absence of NPC1, as well as pharmacological inhibition using U18666A both decreased the extent of lysosome–ER contact sites. Therefore, we hypothesize that the observed Sph block could result from less efficient trafficking across contact sites by other means.

To tease apart the roles of NPC1 as a Sph transporter as opposed to a contact site tether, we made use of a published variant of NPC1 (L472P) which was shown to disrupt the intramolecular lipid transport tunnel (48) but exhibited no change in the cytosolic domains likely used for creating and maintaining organelle contacts. We engineered HeLa 11ht NPC1$^{-/-}$ cell lines to inducibly express either WT or L472P NPC1 protein (*SI Appendix*, Fig. S9*A*). We then investigated lyso-pacSph export in these newly generated cell lines (Fig. 5*C*, quantified in Fig. 5*D*, colocalization images in *SI Appendix*, Fig. S9 *B–D*) and could show that functional NPC1 is able to rescue the Sph accumulation seen in the NPC1 KO cells, whereas the tunnel mutant (L472P) showed prolonged lysosomal staining of the sphingosine probe and consistently higher correlation coefficient across all time points compared to the WT construct. Of note, the Sph accumulation in the NPC1–L472P condition is not as severe as in the NPC1 KO cells, showing that a single point mutation in the intramolecular tunnel delays but not fully blocks lipid exit. This is in line with what was reported for cholesterol (48) and further underlines the likely mechanism that both Sph and cholesterol exit the lysosome through the intermolecular tunnel formed by NPC1.

Finally, we attempted to recreate an NPC1-like phenotype in a WT background by artificially increasing lysosomal lipid levels in order to investigate whether any of the two lipids are preferentially transferred, as hinted by our previous results that NPC1–Sph cross-linking could not be effectively competed out with excess cholesterol (*SI Appendix*, Fig. S3 *E* and *F*). To this end, we synthesized new lysosomally prelocalized probes lyso-Sph and lyso-Chol (Fig. 6*A*). These probes feature the same cage group and lysosomal targeting groups but lack the cross-linkable and clickable groups found in lyso-pacSph and lyso-pacChol. Applying these probes in combination with lyso-pacSph and lyso-pacChol, respectively, allowed us to preload lysosomes with two different lipids at the same time. Upon uncaging, both lipid types were released at the same time, yet we followed only the localization of the lyso-pac-lipids by virtue of their clickable group (schematically illustrated in Fig. 6*B*). Initially, we applied lyso-pacSph together with a 20-fold excess of lyso-Chol to investigate whether Sph

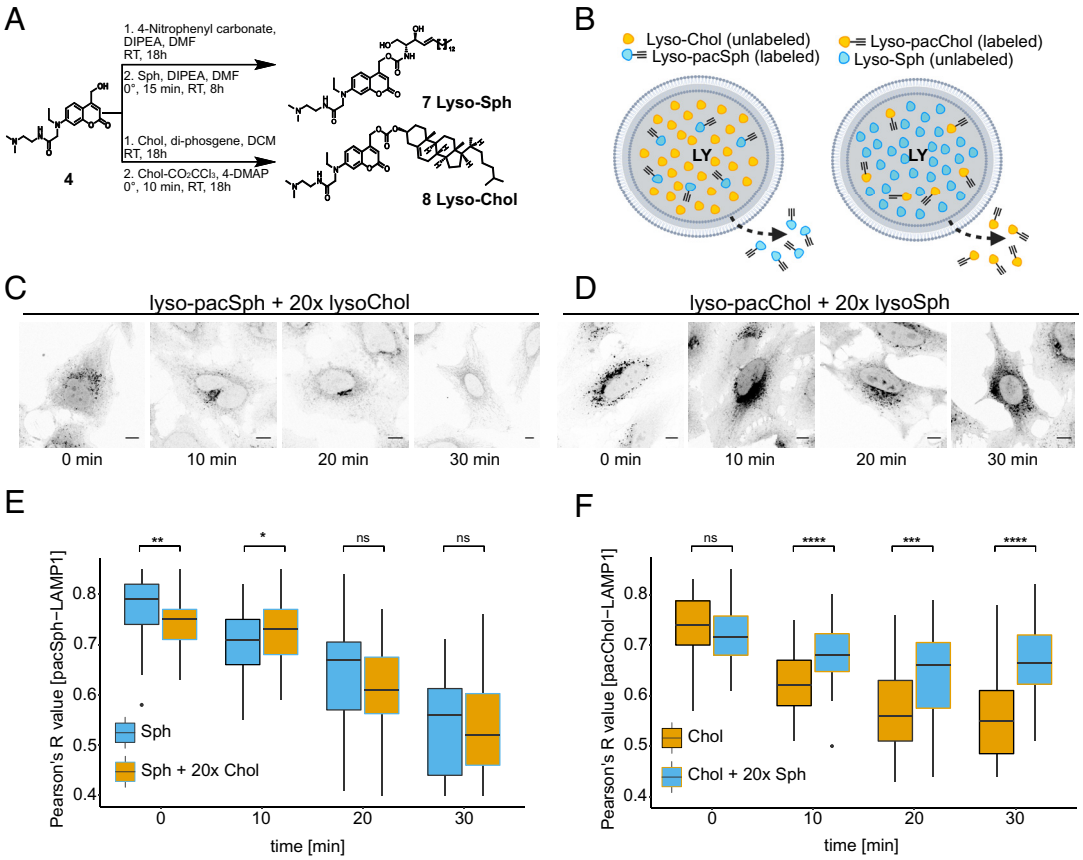


**Fig. 6.** Elevation of lysosomal sphingosine levels can recreate an NPC1-like phenotype. (*A*) Synthesis of lysosome-targeted sphingosine (lyso-Sph, 7) and lysosome-targeted cholesterol (lyso-Chol, 8). (*B*) Illustrative model of the experiment. (*C* and *D*) Confocal images from HeLa WT cells labeled with either lyso-pacSph (1.25 μM) and lyso-Chol (25 μM) (*C*) or lyso-pacChol (750 nM) and lyso-Sph (15 μM) (*D*) for 1 h and chased overnight. Upon uncaging, chase cross-linking experiments were performed from 0 to 30 min. Cells were fixed with methanol and functionalized with AlexaFluor 594 picolyl azide (*C*) or AlexaFluor 488 azide (*D*). (Scale bar, 10 μm.) (*E* and *F*) Quantification of lysosomal lipid egress in *C* and *D*. Pearson's R value of nonthresholded images from lipid channel vs. LAMP1 immunofluorescence calculated for each time point (n ≥ 42) using the Coloc 2 feature from Fiji (ns *P* value > 0.05, **P* value ≤ 0.05, ***P* value ≤ 0.01, ****P* value ≤ 0.001, and *****P* value ≤ 0.0001).

export was delayed in the presence of a large excess of cholesterol (Fig. 6*C*, colocalization in *SI Appendix*, Fig. S10 *A* and *B*). Colocalization analysis between the sphingosine probe and LAMP1 as performed by Pearson's correlation coefficient (Fig. 6*E*) showed no detectable difference in Sph export with or without excess cholesterol. When inverting the experiment, i.e., flooding the lysosome with a 20-fold excess of Sph and following the export of lyso-pacChol, however, we could detect a delay in cholesterol export in the presence of Sph (Fig. 6*D*, quantified in Fig. 6*F*, colocalization in *SI Appendix*, Fig. S10 *C* and *D*). These data further support the hypothesis that the Sph storage phenotype observed in NPC1 $^{-/-}$ cells and to a lesser extent in LIMP-2$^{-/-}$ cells was not a secondary consequence of cholesterol accumulation but rather that increasing lysosomal Sph concentration induced an NPC1/LIMP-2-like delay in cholesterol export, potentially by a preferential interaction of Sph with these proteins. To corroborate this by using genetic manipulations, we employed other cellular models of sphingolipid storage diseases (Niemann–Pick disease type C2 (NPC2$^{-/-}$), Niemann–Pick disease type A (a deficiency of acid sphingomyelinase, SMPD1$^{-/-}$), and sphingosine phosphate lyase insufficiency syndrome (SGPL1$^{-/-}$). As expected, these manipulations resulted in delayed export of the uncaged lyso-pacSph (*SI Appendix*, Fig. S11*A*, quantified in *SI Appendix*, Fig. S11*B*, colocalization images in *SI Appendix*, Fig. S12). Then, we analyzed the export of lyso-pacChol under these conditions (*SI Appendix*, Fig. S11*C*, quantified in *SI Appendix*, Fig. S11*D*, colocalization images in *SI Appendix*, Fig. S13). As expected, NPC2$^{-/-}$ and SMPD1$^{-/-}$ cells stored the cholesterol probe in lysosomes over the entire duration of the experiment. This is consistent with what is observed in cell lines derived from patients suffering from these diseases (8, 49–51) and again supports that Sph and cholesterol export pathways are linked. Interestingly, SGPL1$^{-/-}$ cells do not exhibit delayed cholesterol export and show Pearson coefficients comparable to the WT cell line. This could potentially be due to the subcellular localization of the sphingosine-1-phosphate lyase at the ER. As such, the initial export of Sph and also cholesterol to the limiting lysosomal membrane would function normally (through NPC1/LIMP-2), but failure to utilize the exported Sph at the ER could hinder the further transfer of Sph to the ER, whereas cholesterol would be trafficked and further utilized.

## Discussion

In this study, we combine the concepts of trifunctional lipids with organelle targeting to achieve exquisite spatiotemporal control over these probes. Upon prelocalization of lipids within lysosomes in their caged and therefore inactive state, rapid release by a flash of light provides a synchronized starting point for tightly controlled pulse–trace experiments. This is particularly important for the study of signaling active lipids which are subject to rapid metabolism and degradation. In principle, this design is not restricted to lysosomes. The chemistry required for targeting other organelles such as the plasma membrane, ER, lipid droplets, mitochondria, and Golgi is well established (52) and has even been

applied to the prelocalization of lipids (33–36). The tremendous stability of prelocalized lipids to withstand hydrolytic enzymes in their caged state up to 24 h in this study allowed the optimization of chase times to achieve exclusive organellar localization.

Having optimized the preuncaging localizations of all probes, we applied our lyso-pac-lipids to studying the mechanisms of Sph exit from lysosomes. This is an important step in sphingolipid homeostasis, and it is estimated that the so-called salvage pathway, that is, the reutilization of Sph in sphingolipid biosynthesis, utilizes up to 50 to 90% of the lysosomally derived sphingoid base pool (20, 53). However, to date, the molecular mechanism of lysosome–ER traffic of Sph for not only the salvage but also the SGPL1-dependent breakdown pathway is completely unclear. A recent study in yeast identified an ER–lysosomal tethering protein, Mdm1, which facilitated the incorporation of lysosomal sphinganine into dihydroceramide (54). This points toward a requirement for organelle contact sites in the traffic of Sph and argues for the presence of dedicated Sph transporters, similar to other lipids such as cholesterol (55) or diacylglycerols (56), which depend on the actions of lipid transport proteins such as oxysterol-binding protein (OSBP) or E-Syts for their trafficking between organelles.

To our surprise, our chemoproteomic screen identified two well-known cholesterol-binding proteins, NPC1 and LIMP-2/SCARB2, as Sph interactors. Both proteins have been described to feature hydrophobic cavities ("tunnels") through which cholesterol can pass (11, 14). Interestingly, LIMP-2 was found to bind other lipids besides cholesterol such as phosphatidylserine (PS) (57), hinting a broader specificity. NPC1 on the other hand has not yet been studied with respect to its substrate specificity. However, patients suffering from NPC1 disease feature accumulation of not just cholesterol but multiple lipids within lysosomes including Sph (58). Together with our finding that lyso-pacSph is cross-linked to NPC1, it seems likely that the lipid-binding specificity of NPC1 goes beyond sterols as well. In addition, we observed that NPC1 was pulled down slightly more effectively using the globally distributed pacSph probe, which gave rise to a multitude of (sphingo)lipid metabolites. This could point toward a scenario, where the substrate specificity of NPC1 could even go beyond Sph to include other sphingolipids as well. Based on the structures of both proteins, NPC1 (11) and LIMP-2/SCARB2 (14), we hypothesize that Sph and potentially other lipids could fit into the respective cholesterol-binding pocket.

We then investigated whether NPC1 could not only bind but also traffic Sph out of the lysosomes. The notion of NPC1 as a Sph transporter was proposed following the findings that exogenous addition of Sph could induce an NPC1 phenotype in healthy cells and that pharmacological inhibition of NPC1 in cell culture resulted in sequential elevation of multiple lipids with Sph being the first to accumulate (59). However, other studies featuring pulse–chase experiments with radiolabeled Sph did not find evidence of a Sph trafficking defect in NPC1-deficient cell models (60), potentially because of the hour-long time courses employed. In our hands, several lines of investigations support the hypothesis that NPC1 is capable of trafficking Sph. First, metabolic labeling studies in NPC1$^{-/-}$ showed a delayed postlysosomal metabolism of Sph. Second, visualization of lyso-pacSph revealed a strikingly prolonged lysosomal staining in NPC1$^{-/-}$ cells or by pharmacological induction of an NPC1-like phenotype by U18666A, itraconazole, or posaconazole treatment. In fact, Sph was stained within lysosomes for the entire duration of the experiments, while WT cells cleared all lysosomal lyso-pacSph within 30 min upon uncaging. This could point toward a direct action of NPC1 as a Sph transporter but could also be explained by the well-characterized actions of NPC1 as a contact site tether. In the models employed (NPC1 knockout and U18666A treatment), it was previously shown that lysosome–ER contact sites are drastically reduced (13). As such, the trafficking of Sph to the ER for further incorporation into either the biosynthetic or the salvage pathway would be affected as well. To address this, we employed an NPC1 mutant featuring a point mutation within the hydrophobic lipid trafficking tunnel, while other parts of the proteins (including presumed interaction sites with ER-resident proteins) remain unchanged. This mutant was not able to fully rescue the lysosomal Sph accumulation in an NPC$^{-/-}$ background, highlighting the importance of having a functional lipid trafficking cavity in order to efficiently export Sph.

In addition to uncovering a broader substrate specificity for NPC1, we could also show that NPC1 cross-linking to Sph is not easily displaced by excess cholesterol and that uncaging of an excess of lysosomally prelocalized Sph indeed led to delayed export of cholesterol, whereas the inverse experiment (releasing excess cholesterol) did not cause any delay in Sph export. In addition, most cellular models of sphingolipid storage disorders investigated here showed delayed export of lyso-pacChol as well. Together, these data could suggest that Sph is preferentially trafficked by NPC1 or that the binding of Sph to NPC1 is stronger than that of cholesterol. It is tempting to speculate about a model in which NPC1 is a cholesterol-regulated protein that is able to move other substrates, including Sph, to the limiting membrane of the lysosome for transport at lysosome–ER contact sites (13).

To a lesser extent, a similar concept could apply to LIMP-2. While we did not characterize the Sph–LIMP-2 interaction to the same extent as for NPC1 due to missing tools, we could see an additive effect of the NPC1/LIMP-2 double knockout cells in keeping the uncaged lyso-pacSph in the lysosomes. Future investigations into the function of NPC1 and LIMP-2 as Sph transporters will require reconstitution of the system to accurately investigate binding constants and transport rates to reveal whether indeed Sph binding is stronger than cholesterol and whether addition of Sph would be able to displace cholesterol from the binding cavity.

In conclusion, the presented method to study single lipids with subcellular resolution gave insights into the previously understudied lipid Sph. Similar to cholesterol, Sph interacts with and likely exits the lysosomes via NPC1 and to a lesser extent also via LIMP-2/SCARB2, presumably using their hydrophobic tunnels for delivery to the limiting membrane of the lysosome. From there, it is tempting to speculate that dedicated lipid transport proteins would also shuttle Sph from lysosomes to other organelles at dedicated contact sites. The current dataset did not give hints toward potential interorganellar transporters, potentially because the cross-linking was performed immediately upon uncaging and resident lysosomal proteins were preferentially identified. Owing to the flexibility of our design featuring two photoreactions, this timing could readily be changed to longer intervals to allow for trafficking between organelles to occur in order to capture possible postlysosome Sph transporters. We expect these tools to be broadly applicable not only to the study of sphingolipid export and related diseases and hope that this design sparks the generation of related tools to tackle questions regarding interorganellar transfer of many different lipid species.

## Materials and Methods

**Synthesis of Lipid Probes.** A detailed description of the synthesis and characterization of the lysoprobes can be found in *SI Appendix*.

**Thin-Layer Chromatographic Analysis of Lysosome-Targeted pac-Lipids (Adapted from Refs.** 32 and 61**).** Details can be found in *SI Appendix*. Briefly, cells labeled with 10 μM lysoprobes were UV-irradiated for 90 s on ice with a 405-nm LED lamp. Lipids were extracted from the cell pellet using chloroform/

methanol, clicked to 3-azido-7-hydroxycoumarin (4 μM), and separated by thin layer chromatography. Lipids containing the fluorescent coumarin group were visualized using a gel-doc system.

**Visualization of Clickable Lipids.** Cells grown on coverslips were labeled with the respective concentrations of lyso-pac-lipids and UV-irradiated on ice for 90 s at 405 nm followed by a cross-linking irradiation at 365 nm with a UVP Blak-Ray B100-AP High-Intensity Lamp for 7 min after the respective time periods. For lyso-pacSph, cells were fixed with −20 °C methanol, and noncrosslinked lipids were removed by washing with $CHCl_3$/MeOH/AcOH (10:55:0.75). Cross-linked lipids were labeled with AlexaFluor 594 picolyl azide. For lyso-pacChol, cells were fixed with 4% PFA and 0.1% glyoxal for 20 min at room temperature, solubilized with 0.3% Triton/SDS and blocked overnight. Cross-linked lipids were labeled with AlexaFluor 488 picolyl azide and subjected to immunofluorescence experiments. Images were acquired using a confocal laser scanning microscope (Zeiss LSM800) with a 63× oil objective. Images were further analyzed using ImageJ 2.1.0/1.53c. The Pearson coefficient for analysis of signal distribution within cells and lysosomes was extracted from the raw images with Coloc 2 plugin.

**Cell Labeling, Cross-Linking, and Pulldown for Protein–Lipid Interaction Studies.** A detailed protocol can be found in *SI Appendix*. Briefly, cells were labeled with lyso-pacSph (5 μM), lyso-pacChol (10 μM), or their uncaged counterpart pacSph (1 μM) or pacChol (10 μM) for the times indicated in the respective figures. The lysoprobes were subsequently uncaged at 405 nm for 90 s and then immediately irradiated at 365 nm with a UVP Blak-Ray B100-AP High-Intensity Lamp for 10 min. The lysate was adjusted for protein concentration and subjected to click reaction (500 μM $CuSO_4$, 50 μM Tris (benzyltriazolylmethyl) amine (TBTA), 500 μM ascorbic acid, and 250 μM picolyl azide-PEG4-biotin) for 1 h at 37 °C. Subsequently, proteins were precipitated twice by chloroform/methanol precipitation. For enrichment of the lipid–protein complexes, streptavidin sepharose beads were used, and the proteins were eluted using 1% NP40, 0.4% SDS, and 2 mM biotin for 5 min at 98 °C. Probes were either subjected to SDS-PAGE followed by western blot analysis or submitted to liquid chromatography followed by tandem mass spectrometry (LC-MS/MS) analysis.

**LC-MS/MS Analysis and Mass Spectrometric Data Analysis.** Details can be found in *SI Appendix*. Briefly, enriched protein–lipid complexes were subjected to an in-solution tryptic digest, followed by tandem mass tag (TMT) labeling. TMT-labeled peptides were mixed and purified by a reverse-phase clean-up step and were analyzed by LC-MS/MS. Acquired data were analyzed using IsobarQuant (62) and Mascot V2.4. Only proteins that were quantified with at least two unique peptides were considered for the analysis. The raw TMT reporter ion signals were first cleaned for batch effects using limma (63) and further normalized using variance stabilization normalization (64). Proteins were tested for differential expression using the limma package. A protein was annotated as a hit with a false discovery rate <0.01 and a fold change of >1.5. Hit proteins were clustered on the Euclidean distance between signal sums normalized by the respective no UV condition. The data have been deposited to the ProteomeXchange Consortium via the PRIDE (65) partner repository with the dataset identifier PXD039780.

**Data, Materials, and Software Availability.** Proteomics Data have been deposited in PRIDE to the ProteomeXchange Consortium via the PRIDE (66) partner repository with the dataset identifier PXD039780. All other data are included in the article and/or *SI Appendix*.

**ACKNOWLEDGMENTS.** We thank Wim Annaert (Katholieke Universiteit (KU) Leuven) for providing the HeLa NPC1$^{-/-}$ cell line, Britta Brügger (Heidelberg University) for providing the HeLa SGPL1$^{-/-}$ cell line, and Alain Townsend (University of Oxford) for the NPC2$^{-/-}$ and SMPD1$^{-/-}$ cell lines. The work of J.A., J.N., P. Hempelmann and D.H. was funded by the Deutsche Forschungsgemeinschaft (DFG, German Research Foundation, project number 112927078–TRR83 and project number 278001972 – TRR 186), and the work of P.S. was supported by the Deutsche Forschungsgemeinschaft (DFG Research Group 2625; SA683/10-1).

Author affiliations: [a]Heidelberg University Biochemistry Center, Ruprecht-Karls-Universität Heidelberg, 69120 Heidelberg, Germany; [b]European Molecular Biology Laboratory, 69117 Heidelberg, Germany; and [c]Institute of Biochemistry, Christian-Albrechts-Universität Kiel, 24118 Kiel, Germany

1. A. Ballabio, J. S. Bonifacino, Lysosomes as dynamic regulators of cell and organismal homeostasis. *Nat. Rev. Mol. Cell Biol.* **21**, 101–118 (2020).
2. F. M. Platt, Emptying the stores: Lysosomal diseases and therapeutic strategies. *Nat. Rev. Drug Discov.* **17**, 133–150 (2018).
3. A. R. A. Marques, P. Saftig, Lysosomal storage disorders – challenges, concepts and avenues for therapy: Beyond rare diseases. *J. Cell Sci.* **132**, jcs221739 (2019).
4. M. S. Brown, J. L. Goldstein, A receptor-mediated pathway for cholesterol homeostasis. *Science* **1979**, 34–47 (1986).
5. J. L. Goldstein, R. A. DeBose-Boyd, M. S. Brown, Protein sensors for membrane sterols. *Cell* **124**, 35–46 (2006).
6. C. Thiele, J. Spandl, Cell biology of lipid droplets. *Curr. Opin. Cell Biol.* **20**, 378–385 (2008).
7. S. Xu, B. Benoff, H. L. Liou, P. Lobel, A. M. Stock, Structural basis of sterol binding by NPC2, a lysosomal protein deficient in Niemann-Pick type C2 disease. *J. Biol. Chem.* **282**, 23525–23531 (2007).
8. R. E. Infante *et al.*, NPC2 facilitates bidirectional transfer of cholesterol between NPC1 and lipid bilayers, a step in cholesterol egress from lysosomes. *Proc. Natl. Acad. Sci. U.S.A.* **105**, 15287–15292 (2008).
9. M. Nguyen Trinh, M. S. Brown, J. Seemann, J. L. Goldstein, F. Lu, Lysosomal cholesterol export reconstituted from fragments of Niemann-Pick C1. *Elife* **7**, 1–14 (2018).
10. Y. Meng, S. Heybrock, D. Neculai, P. Saftig, Cholesterol handling in lysosomes and beyond. *Trends Cell Biol.* **30**, 452–466 (2020).
11. M. B. L. Winkler *et al.*, Structural Insight into Eukaryotic sterol transport through Niemann-pick Type C proteins. *Cell* **179**, 485–497.e18 (2019).
12. X. Du *et al.*, A role for oxysterol-binding protein-related protein 5 in endosomal cholesterol trafficking. *J. Cell Biol.* **192**, 121–135 (2011).
13. D. Höglinger *et al.*, NPC1 regulates ER contacts with endocytic organelles to mediate cholesterol egress. *Nat. Commun.* **10** (2019).
14. D. Neculai *et al.*, Structure of LIMP-2 provides functional insights with implications for SR-BI and CD36. *Nature* **504**, 172–176 (2013).
15. S. Heybrock *et al.*, Lysosomal integral membrane protein-2 (LIMP-2/SCARB2) is involved in lysosomal cholesterol export. *Nat Commun* **10** (2019).
16. V. Schoop, A. Martello, E. R. Eden, D. Höglinger, Cellular cholesterol and how to find it. *Biochim. Biophys. Acta Mol. Cell Biol. Lipids* **1866**, 158989 (2021).
17. A. H. Futerman, H. Riezman, The ins and outs of sphingolipid synthesis. *Trends Cell Biol.* **15**, 312–318 (2005).
18. Y. A. Hannun, L. M. Obeid, Principles of bioactive lipid signalling: Lessons from sphingolipids. *Nat. Rev. Mol. Cell Biol.* **9**, 139–150 (2008).
19. Y. A. Hannun, R. M. Bell, Functions of sphingolipids and sphingolipid breakdown products in cellular regulation. *Science* **1979**, 500–507 (1989).
20. K. Kitatani, J. Idkowiak-Baldys, Y. A. Hannun, The sphingolipid salvage pathway in ceramide metabolism and signaling. *Cell Signal* **20**, 1010–1018 (2008).
21. M. Bektas *et al.*, Sphingosine 1-phosphate lyase deficiency disrupts lipid homeostasis in liver. *J. Biol. Chem.* **285**, 10880–10889 (2010).
22. P. Haberkant *et al.*, Bifunctional sphingosine for cell-based analysis of protein-sphingolipid interactions. *ACS Chem. Biol.* **11**, 222–230 (2016).
23. S. Bockelmann *et al.*, A search for ceramide binding proteins using bifunctional lipid analogs yields CERT-related protein StarD7. *J. Lipid Res.* **59**, 515–530 (2018).
24. R. E. Pagano, R. Watanabe, C. Wheatley, M. Dominguez, *Applications of BIODIPY-Sphingolipid Analogs to Study Lipid Traffic and Metabolism in Cells* (Elsevier Masson SAS, 2000).
25. G. Schwarzmann, C. Arenz, K. Sandhoff, Labeled chemical biology tools for investigating sphingolipid metabolism, trafficking and interaction with lipids and proteins. *Biochim. Biophys. Acta Mol. Cell Biol. Lipids* **1841**, 1161–1173 (2014).
26. R. G. Ashcroft, K. R. Thulborn, J. R. Smith, H. G. L. Coster, W. H. Sawyer, Perturbations to lipid bilayers by spectroscopic probes as determined by dielectric measurements. *Biochim. Biophys. Acta Biomembr.* **602**, 299–308 (1980).
27. A. Chattopadhyay, Chemistry and biology of N-(7-nitrobenz-2-oxa-1,3-diazol-4-yl)-labeled lipids: Fluorescent probes of biological and model membranes. *Chem. Phys. Lipids* **53**, 1–15 (1990).
28. O. Maier, V. Oberle, D. Hoekstra, Fluorescent lipid probes: Some properties and applications (a review). *Chem. Phys. Lipids* **116**, 3–18 (2002).
29. P. Haberkant *et al.*, In vivo profiling and visualization of cellular protein-lipid interactions using bifunctional fatty acids. *Angew. Chem. - Int. Ed.* **52**, 4033–4038 (2013).
30. J. J. Hulce, A. B. Cognetta, M. J. Niphakis, S. E. Tully, B. F. Cravatt, Proteome-wide mapping of cholesterol-interacting proteins in mammalian cells. *Nat. Methods* **10**, 259–264 (2013).
31. D. Höglinger, A. Nadler, C. Schultz, Caged lipids as tools for investigating cellular signaling. *Biochim. Biophys. Acta Mol. Cell Biol. Lipids* **1841**, 1085–1096 (2014).
32. D. Höglinger *et al.*, Trifunctional lipid probes for comprehensive studies of single lipid species in living cells. *Proc. Natl. Acad. Sci. U.S.A.* **114**, 1566–1571 (2017).
33. A. Nadler *et al.*, Exclusive photorelease of signalling lipids at the plasma membrane. *Nat. Commun.* **6**, 1–10 (2015).
34. N. Wagner, M. Stephan, D. Höglinger, A. Nadler, A click cage: Organelle-specific uncaging of lipid messengers. *Angew. Chem. - Int. Ed.* **57**, 13339–13343 (2018).
35. S. Feng *et al.*, Lysosome-targeted photoactivation reveals local sphingosine metabolism signatures. *Chem. Sci.* **10**, 2253–2258 (2019).
36. S. Feng *et al.*, Mitochondria-specific photoactivation to monitor local sphingosine metabolism and function. *Elife* **7**, 1–23 (2018).
37. A. M. Kaufmann, J. P. Krise, Lysosomal sequestration of amine-containing drugs: Analysis and therapeutic implications. *J. Pharm. Sci.* **96**, 729–746 (2007).

38. M. J. Gerl *et al.*, Sphingosine-1-phosphate lyase deficient cells as a tool to study protein lipid interactions. *PLoS One* **11**, e0153009 (2016).
39. H. J. Kwon *et al.*, Structure of N-terminal domain of NPC1 reveals distinct subdomains for binding and transfer of cholesterol. *Cell* **137**, 1213–1224 (2009).
40. J. Li, S. R. Pfeffer, Lysosomal membrane glycoproteins bind cholesterol and contribute to lysosomal cholesterol export. *Elife* **5**, e21635 (2016), 10.7554/eLife.21635.001.
41. A. K. Tharkeshwar *et al.*, A novel approach to analyze lysosomal dysfunctions through subcellular proteomics and lipidomics: The case of NPC1 deficiency. *Sci. Rep.* **7**, 1–20 (2017).
42. M. Hölttä-Vuori *et al.*, BODIPY-cholesterol: A new tool to visualize sterol trafficking in living cells and organisms. *Traffic* **9**, 1839–1849 (2008).
43. E. D. Carstea, Niemann-pick C1 disease gene: Homology to mediators of cholesterol homeostasis. *Science (1979)* **370**, 1 (1996).
44. P. Saha *et al.*, Inter-domain dynamics drive cholesterol transport by NPC1 and NPC1L1 proteins. *bioRxiv* **3**, 1–28 (2020).
45. F. Lu *et al.*, Identification of NPC1 as the target of U18666A, an inhibitor of lysosomal cholesterol export and Ebola infection. *Elife* **4**, 1–16 (2015).
46. T. Long *et al.*, Structural basis for itraconazole-mediated NPC1 inhibition. *Nat. Commun.* **11**, 152 (2020).
47. M. N. Trinha *et al.*, Triazoles inhibit cholesterol export from lysosomes by binding to NPC1. *Proc. Natl. Acad. Sci. U.S.A.* **114**, 89–94 (2017).
48. L. Vanharanta *et al.*, High-content imaging and structure-based predictions reveal functional differences between Niemann-Pick C1 variants. *Traffic* **21**, 386–397 (2020).
49. M. M. McGovern *et al.*, Lipid abnormalities in children with types A and B Niemann Pick disease. *J. Pediatrics* **145**, 77–81 (2004).
50. E. H. Schuchman, M. P. Wasserstein, Types A and B Niemann-Pick disease. *Best Pract. Res. Clin. Endocrinol. Metab.* **29**, 237–247 (2015).
51. D. C. Ko, J. Binkley, A. Sidow, M. P. Scott, The integrity of a cholesterol-binding pocket in Niemann-Pick C2 protein is necessary to control lysosome cholesterol levels. *Proc. Natl. Acad. Sci. U.S.A.* **100**, 2518–2525 (1999).
52. W. Xu, Z. Zeng, J. H. Jiang, Y. T. Chang, L. Yuan, Discerning the chemistry in individual organelles with small-molecule fluorescent probes. *Angew. Chem. - Int. Ed.* **55**, 13658–13699 (2016).
53. B. K. Gillard, R. G. Clement, D. M. Marcus, Variations among cell lines in the synthesis of sphingolipids in de novo and recycling pathways. *Glycobiology* **8**, 885–890 (1998).
54. V. Girik, S. Feng, H. Hariri, M. Henne, H. Riezman, Vacuole-specific lipid release for tracking intracellular lipid metabo-lism and transport in Saccharomyces cerevisiae. bioRxiv [Preprint] (2021). https://doi.org/10.1101/2021.05.04.442581 (Accessed 4 May 2021).
55. B. Antonny, J. Bigay, B. Mesmin, The oxysterol-binding protein cycle: Burning off PI(4)P to transport cholesterol. *Annu. Rev. Biochem.* **87**, 809–837 (2018).
56. Y. Saheki *et al.*, Control of plasma membrane lipid homeostasis by the extended synaptotagmins. *Nat. Cell Biol.* **18**, 504–515 (2016).
57. K. S. Conrad *et al.*, Lysosomal integral membrane protein-2 as a phospholipid receptor revealed by biophysical and cellular studies. *Nat. Commun.* **8**, 1908 (2017).
58. C. Rodriguez-Lafrasse, R. Rousson, P. G. Pentchev, P. Louisot, M. T. Vanier, Free sphingoid bases in tissues from patients with type C Niemann-Pick disease and other lysosomal storage disorders. *BBA – Mol. Basis of Disease*, 138–144 (1994).
59. E. Lloyd-Evans *et al.*, Niemann-Pick disease type C1 is a sphingosine storage disease that causes deregulation of lysosomal calcium. *Nat. Med* **14**, 1247–1255 (2008).
60. T. Blom, Z. Li, R. Bittman, P. Somerharju, E. Ikonen, Tracking sphingosine metabolism and transport in Sphingolipidoses: NPC1 deficiency as a test case. *Traffic* **13**, 1234–1243 (2012).
61. C. Thiele, K. Wunderling, P. Leyendecker, Multiplexed and single cell tracing of lipid metabolism. *Nat. Methods* **16**, 1123–1130 (2019).
62. H. Franken *et al.*, Thermal proteome profiling for unbiased identification of direct and indirect drug targets using multiplexed quantitative mass spectrometry. *Nat. Protoc.* **10**, 1567–1593 (2015).
63. M. E. Ritchie *et al.*, Limma powers differential expression analyses for RNA-sequencing and microarray studies. *Nucleic Acids Res.* **43**, e47 (2015).
64. W. Huber, A. Von Heydebreck, H. Sültmann, A. Poustka, M. Vingron, Variance stabilization applied to microarray data calibration and to the quantification of differential expression. *Bioinformatics* **18** (2002).
65. Y. Perez-Riverol *et al.*, The PRIDE database resources in 2022: A Hub for mass spectrometry-based proteomics evidences. *Nucleic Acids Res.* **50**, D543–D552 (2022).
66. J. Notbohm, P. Haberkant, F. Stein, D. Höglinger, Identification of proteins crosslinked to lysosomal sphingosine and cholesterol probes. *PRIDE*. https://www.ebi.ac.uk/pride/archive/projects/PXD039780. Deposited 1 February 2023.